Development of a Mechanistic Foam Simulator: The Population Balance and Generation by Snap-Off

A.H. Falls, SPE, Shell Development Co.
G.J. Hirasaki, SPE, Shell Development Co.
T.W. Patzek, SPE, Shell Development Co.
D.A. Gauglitz,* Shell Development Co.
D.D. Miller,** SPE, Shell Development Co.
T. Ratulowski,† Shell Development Co.

Summary. The mobility of a foam depends heavily on its texture, which is the distribution of bubble sizes in the dispersion. To incorporate this variable in a mechanistic simulator, the usual conservation equations are coupled with balances on the densities of flowing and stationary bubbles in the foam. This approach to modeling foam flow is illustrated with a simulation of a displacement in which foam is generated in situ by capillary snap-off.

Introduction

Many EOR schemes use gases; steamdrives and CO_2 floods are well-known examples. Although such processes can be highly efficient when stabilized by gravity or unique permeability distributions, they ordinarily exhibit poor volumetric sweep efficiencies. Gases have mobilities that are much higher than those of liquids and thus tend to override or to channel through oil in a formation. This decreases the amount of oil that the gas contacts as well as the time for gas to break through to producing wells.

A gas displacement process can be improved if the mobility of the gas can be decreased. As laboratory[1-3] and field[3] studies have demonstrated, one way to do this is to disperse the gas as a foam in a continuous liquid phase. In fact, foams are so effective in controlling gas mobility that they not only hold promise for steam and CO_2 processes but may one day control injection profiles and serve as drive fluids for surfactant and caustic slugs.

Despite the potential of foams in oil recovery, however, a model that can describe and predict their flow through porous media has yet to be developed. To this end, we have examined aqueous foams as they moved through simple porous media without oil present. From this work, we have identified some of the factors governing the rheology, generation, and destruction of foams in pore space. This paper describes these mechanisms and demonstrates how mathematical models for them can be incorporated into a simulator. This mechanistic simulator could ultimately be used to calibrate simpler, phenomenological simulations or to interpret and design field-scale displacements.

Basic Concepts

Definition of Foam in Porous Media. The structure of foam inside a porous medium can differ from that of the "bulk" or "polyhedral" foams commonly encountered as dishwashing suds and shaving creams. To avoid confusion, we have defined foam inside a porous medium as a dispersion of gas in a liquid such that the liquid phase is continuous (i.e., connected) and at least some part of the gas is made discontinuous by thin liquid films called lamellae.

This definition encompasses both bulk foams, in which the average bubble size is much smaller than the dimensions of the pore space, and so-called individual-lamellae foams,[4] in which the bubble size exceeds the pore size. The lamellae may be short-lived, as in the foams called "unstable."[5] In these, the flow of gas is impeded by foam films that "break and then reform."[6] Lamellae may also be longer-lived and translate from pore to pore.[4,5]

Types of Foams in Porous Media. Within this definition, there are two classes of foams. The first is a "continuous-gas" foam (Fig. 1), in which there exists at least one gas channel that is continuous (i.e., uninterrupted by lamellae) over a macroscopic portion of the sample. Foam lamellae are present but are stationary and simply prevent gas from flowing through part of the pore network. Thus, gas can flow through the pore network without having to displace lamellae. The second is called a "discontinuous-gas" foam (Fig. 2), in which all the gas phase is made discontinuous by lamellae and there are no gas channels that are continuous over large distances. For gas to flow, lamellae must be transported through the pore system.

How Foam Influences Phase Mobilities

Effects on Liquid Mobility. In a water-wet porous medium, the liquid-phase relative mobility does not depend on whether the gas exists as a foam.[7,8] Most of the liquid resides either in smaller pores, which do not contain gas, or next to the solid in pores that are occupied by both phases. As long as the amount of liquid carried in lamellae is small compared with the total flux of liquid, the mobility of the liquid can be taken as the usual function of its saturation.

How Foam Reduces Gas Mobility. The ways that foam reduces gas mobility can be understood from the simple diagram of Fig. 1. If a portion of the gas phase is continuous (Fig. 1), foam diminishes the cross-sectional area through which gas is able to flow. We consider this to be strictly a relative permeability effect, the foam creating a large effective trapped-gas saturation.

On the other hand, when all the gas phase is discontinuous (Fig. 2), not only can its relative permeability be smaller, but it appears to have a larger viscosity. For gas to flow, lamellae must be forced through the pore network.

Relative Permeability Effects. The variables that affect the relative permeability of gas in a foam have not yet been conclusively identified. As mentioned above, we believe gas relative permeability to be proportional to the area through which gas flows. The area through which gas flows should, in turn, depend on the pressure gradient and the density of stationary bubbles (texture). The gas relative permeability can increase only if the pressure gradient is large enough to mobilize stationary lamellae.

Constituents of Apparent Gas Viscosity. By contrast, a theory for the apparent gas viscosity of foams in simple porous media has

*Now at Chevron Oil Field Research Co.
**Now at Kodak.
†Now at the U. of Notre Dame.

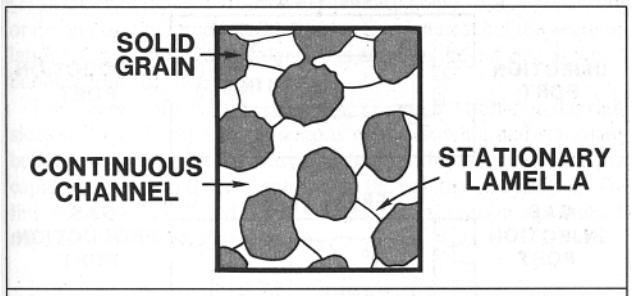

Fig. 1—Sketch of a continuous-gas foam.

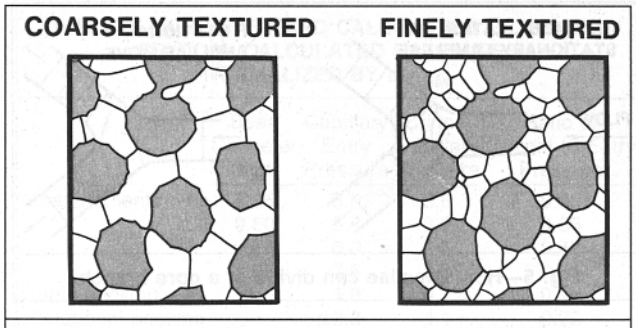

Fig. 2—Representations of discontinuous-gas foams.

already been adduced.[9] It embodies the mechanisms that resist the transport of lamellae through constricted pore channels. This resistance is made up of two components: the resistance from flow through smooth, uniform pores,[4] μ_s, and that resulting from constrictions. When the average bubble density in the flowing phase is less than the density of pore constrictions and $k_{rg} \ll 1$, measured apparent viscosities are well correlated by

$$\mu_{g,\text{app}} = \mu_s + G\sigma n_L r/v_g. \quad \ldots\ldots\ldots\ldots\ldots\ldots\ldots\ldots\ldots\ldots (1)$$

The apparent viscosity of foam in porous media depends strongly on the texture of the foam.[2,4,9] The finer the texture, the larger the number of lamellae that must be transported through the system (see Fig. 2). Fig. 3 shows just how important bubble size can be. It displays the apparent viscosity of foams made from a 1 wt% aqueous solution of Siponate DS-10,™ a commercial sodium dodecylbenzenesulfonate, in homogeneous bead packs as it depends on the ratio of foam-bubble size to the equivalent capillary radius of the porous medium. For these measurements, gas fractional flow, interstitial velocity, and relative permeability were about 0.99, 0.7 cm/s [0.3 in./sec], and 0.06, respectively, and foam-bubble size did not change in situ. If the ratio of bubble size to average pore size diminishes two-fold, the apparent gas viscosity increases by an order of magnitude.

Mechanisms That Influence Foam Texture

Foam Texture Can Change Within a Porous Medium. Although gas mobility depends heavily on foam texture, this parameter would not have to be treated as a variable in modeling foam flow if it never changed within porous media. Texture, however, can change abruptly in situ.

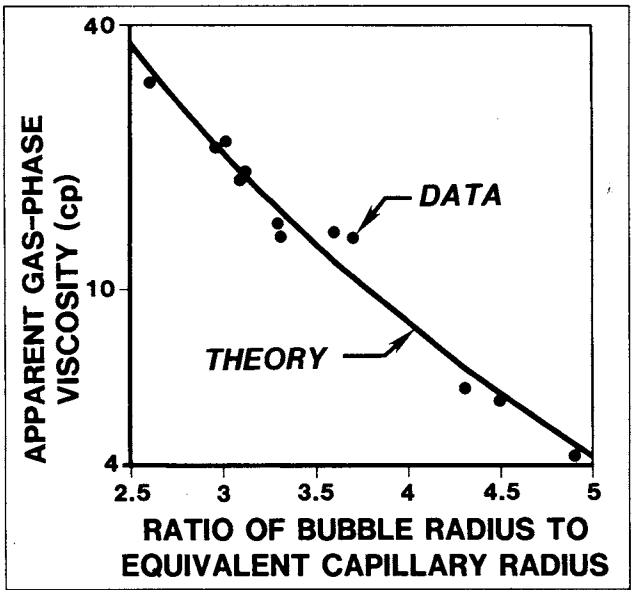

Fig. 3—Apparent viscosity of foams in homogeneous bead packs.

There are many simple experiments that can be performed to show how texture can be altered by porous media. One example occurs when surfactant solution is drained from a vertical, homogeneous bead pack. One such system consisted of 64 cm [25 in.] of 20/30-mesh glass beads packed in a 91-cm [3-ft] section of a 2.5-cm [1-in.] -diameter glass tube. A screen above a rubber stopper in the lower end of the tube retained the beads. The flow of surfactant solution was regulated by a stopcock connected to the bottom of the pack by 0.64-cm [¼-in.] -diameter glass tubing.

If the stopcock is slightly opened, liquid drains steadily from the bottom of the system as air invades from the top. Above the 100% liquid level, a continuous-gas foam is created because some of the liquid left behind exists as stationary lamellae. If, on the other hand, the stopcock is opened fully, liquid flows out steadily until gas reaches the packed section. Once gas enters the beads, moving lamellae are formed and the flow of liquid from the system slows and becomes intermittent. In this case, the increased gas velocity creates a discontinuous-gas foam that almost completely plugs the pack.

Thus, foam texture not only governs foam mobility but can vary within pore space. That the results of a particular experiment appear independent of the texture that is *injected* doesn't mean that this variable is unimportant. Instead, when injected texture appears unimportant, it is likely that the porous medium is altering it very quickly.

Some of the mechanisms that alter texture in situ have been identified as capillary snap-off, division, coalescence, and mass transfer between bubbles caused by diffusion or condensation and evaporation. Each of these is described below.

Capillary Snap-Off. Snap-off, first described by Roof[9] as a mechanism that traps oil during waterflooding, can generate foam lamellae when the nonwetting phase is a gas.[5] How snap-off occurs is illustrated by the diagram of a constricted capillary shown in Fig. 4. The walls of the tube are wet by surfactant solution, and gas flows through the system from left to right. If the mean curvature of the gas/liquid interface in the constriction is greater than that in the rest of the capillary (and the wetting films are thick compared with the distance of molecular interactions), the capillary pressure in the neck is higher than anywhere else. If the pressure gradient in the gas phase is negligible, this means that the liquid-phase pres-

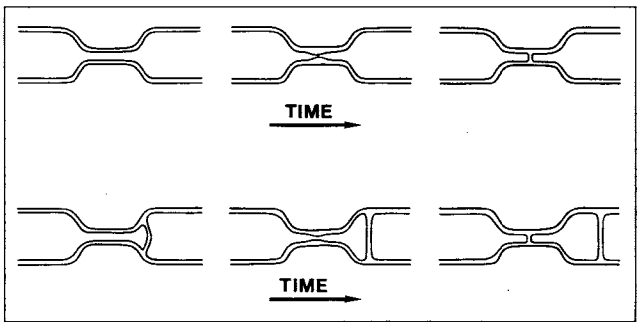

Fig. 4—How capillary snap-off can generate foam lamellae in a constricted capillary tube.

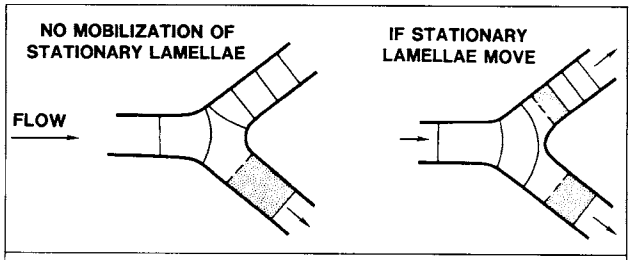

Fig. 5—How lamellae can divide at a pore branch.

sure is lower in the neck than in the rest of the capillary. Consequently, liquid flows into the constriction and accumulates there in a collar. The collar can grow, become unstable, and bridge across the constriction, thereby forming a lamella. After the newly formed lamella exits, other bubbles can be generated.

The same mechanism operates inside the porous media, where it is aided by local heterogeneities. For snap-off to occur, the capillary pressure must be sufficiently low (liquid saturation high). A model for the rate at which lamellae are generated by snap-off is presented later.

Division. Another way that foam lamellae can be generated is by division.[5] Division is the mechanism responsible for forming the discontinuous-gas foam in the gravity-drainage experiment detailed previously. Unlike capillary snap-off, division requires that some lamellae already be present and mobile.

Fig. 5 represents how division can occur at a fork in a flow path. If stationary lamellae block flow through one branch, lamellae merely flow through the other side. Foam texture is unchanged. That is, the bubble size that exits from the system is the same as the size that enters it. By contrast, if the pressure gradient is large enough to mobilize lamellae in both branches simultaneously, lamellae divide. When division occurs, the texture of foam emerging from the system is nonuniform and is finer than the texture that enters the pore branch. Consequently, division is a mechanism that can modify foam texture within porous media.

Although division has not yet been described mathematically, the rate at which bubbles subdivide ought to depend on the pressure gradient and the number of pore branches within the system. Moreover, generation by division (up to some limit) should be proportional to the density of flowing bubbles and gas velocity: the more rapidly lamellae are delivered to sites for division, the faster new bubbles can be created.

Coalescence. Foam-bubble density decreases when lamellae rupture. Undoubtedly, many factors affect the stability of foams in porous media. Among these are the thermodynamic (meta)stability of lamellae, for which capillary pressure is an important parameter; the hydrodynamics of lamella thinning; the kinetics of film rupture; the dampening of thermally and mechanically induced waves by adsorbed surfactant layers; the elasticity of lamellae; the presence and spreading of oil films at gas/water interfaces; and the adsorbing of surfactant at the interfaces of water/oil emulsions. Stationary and moving lamellae may rupture by different mechanisms.

Mass Transfer Between Bubbles. Another way in which foam-bubble density can diminish is by mass transfer between bubbles. In foams made from noncondensable gases, this occurs by pressure-driven diffusion. Because the pressure in a smaller bubble can be greater than that in a larger one, large bubbles can grow at the expense of smaller ones as mass is transferred through lamellae. Pressure-driven diffusion can be a fairly slow process, especially if the gas is relatively insoluble and has a low diffusivity in water.

In foams made from condensable gases, such as steam foams, mass can be transferred between bubbles by evaporation and condensation. This change of phase is ordinarily more rapid than diffusion and can quickly destroy foams outside porous media. In fact, steam foams are often formulated with a small amount of noncondensable gas to stabilize them to condensation and evaporation.[10]

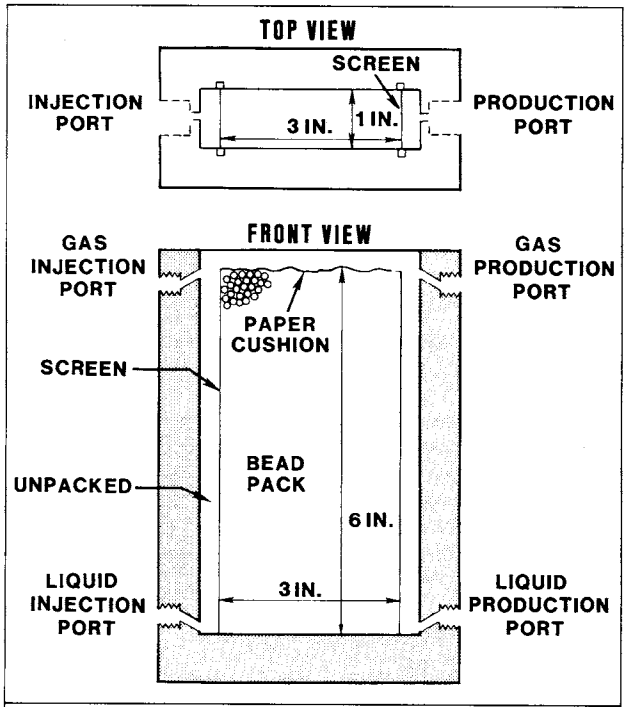

Fig. 6—Sketch of bead packs for which capillary entry pressures and critical capillary pressures for snap-off were measured.

Modeling Foam Flow Through Porous Media: Population-Balance Approach

Because texture greatly influences foam mobility and can change abruptly within pore space, its effects must be included in a simulator. We do it by augmenting the usual equations of mass, momentum, and energy conservation with balances for the average number density of flowing and stationary bubbles within the foam. These new equations account for changes in foam texture caused by mechanisms that create and destroy bubbles in situ. They also allow for transfer of bubbles between the flowing and stationary gas phases (trapping and mobilization).

The general, volume-averaged population balances for flowing and stationary bubbles are a pair of coupled, nonlinear, integro-differential equations akin to Boltzmann's equation in the kinetic theory of gases or to the Payatakes *et al.*[11] equations of oil ganglia dynamics. The derivation of these, detailed elsewhere,[12] follows well-developed population-balance methods.

To render the general equations tractable, they are expanded in moments of the bubble-size distribution. Only the zeroth-order moments, which describe the average number densities of flowing and stationary bubbles, and the first-order moments, which together describe conservation of gas, are retained. The expressions for the evolution of the average bubble densities (n_f and n_s, the number of bubbles per unit volume of flowing and stationary gas, respectively) have the same form as the equations governing conservation of mass and energy:

$$\frac{\partial}{\partial t}(\phi S_g x_f n_f) = -\nabla\cdot(u_{gD} n_f - J_K) + D_f - \theta + q_{bf} \quad \ldots\ldots\ldots (2)$$

and

$$\frac{\partial}{\partial t}[\phi S_g (1-x_f) n_s] = D_s + \theta + q_{bs}. \quad \ldots\ldots\ldots\ldots\ldots\ldots (3)$$

Eq. 2 states that the rate of change in flowing bubble density within a control volume of the medium is equal to the net convection of bubbles into the volume plus the rate at which bubbles are added to the flowing phase within this volume. The latter can be a result

of (1) bubbles disappearing because of mass transfer between them, (2) transfer of lamellae from the stationary phase, or (3) generation or destruction of lamellae. Similarly, Eq. 3 states that the accumulation of stationary bubble density is equal to the net rate at which bubbles join the stationary phase.

The fraction of gas that is flowing, x_f, and the terms on the right sides of Eqs. 2 and 3 are functions of the flowing and stationary bubble densities as well as variables (e.g., velocity, saturation, and capillary pressure) that are external to the population balances. The link between Eqs. 2 and 3 and the usual conservation equations is the gas mobility in Darcy's law,

$$u_{gD} = -\lambda_{rg}(n_f, x_f, \ldots)k\nabla\Phi_g. \quad \ldots\ldots\ldots\ldots\ldots\ldots\ldots\ldots (4)$$

So, the idea is simple. We build into Darcy's law the way bubble densities affect gas viscosity and relative permeability and use the population balances to track the bubble densities. This approach models displacements in which lamellae "make and break" or translate from pore to pore equally well. Even when foams are stable, lamellae can be continuously generated and destroyed in situ. Thus, the difference between foams is one of degree. Foams that are unstable have large average bubble sizes and small gas-mobility reductions. As lamellae become longer-lived, the average bubble size becomes smaller and the gas-mobility reduction greater. The population balances account for this.

For this approach to succeed in modeling foam flow, mathematical models for gas mobility and generation and loss mechanisms must be developed. In the next sections, we adduce a model for generation by capillary snap-off and then illustrate how the population-balance equations can be used to simulate foam displacements.

Model for Generation by Capillary Snap-Off

Mast[5] observed foam bubbles forming and coalescing in glass micromodels. Small bubbles were made by what we call snap-off near the outflow end of his models as gas flowed from a tighter section into a region of larger pores. Here we quantify this mechanism.

Critical Capillary Pressure for Snap-Off. Roof[9] has shown that snap-off can make a nonwetting phase discontinuous only if the capillary pressure is below a critical value. This criterion applies to gas bubbles in porous media.

Experimental. We measured capillary entry pressures and critical capillary pressures for snap-off for several sizes of glass beads packed in a transparent model (see Fig. 6). The entry and exit to the pack consisted of cavities separated from the beads by screens whose openings were larger than the pore size. Gas and liquid were introduced and removed through separate ports. The capillary pressure at the top of the pack was determined from the distance between the top of the pack and the liquid level in the entry or exit section.

The pack was saturated with a 1 wt% aqueous solution of Siponate DS-10. Gas was injected while liquid was produced. The capillary entry pressure was determined from the liquid level in the entry when gas first entered the pack.

The critical capillary pressure for snap-off was next measured by monitoring the liquid level in the outflow section. While gas was being injected, bubbles appeared at the outflow end from the time gas broke through until the liquid level in the outflow section dropped below what corresponded to the critical capillary pressure. Below this level, gas exited from the pack as a continuous phase. That is, foam bubbles were not generated as gas left the system.

This value of the critical capillary pressure was then checked by shutting in the liquid production port, opening the gas production port, and injecting liquid. Liquid levels in the entry and exit sections rose. At some level, the gas leaving the pack no longer flowed as a continuous phase. That is, bubbles were again created as gas exited the system. The two ways of measuring the critical capillary pressure for snap-off were in accord.

Theoretical. To correlate the measured capillary entry and critical capillary pressures, the porous media are regarded as cubic and hexagonal packings of spheres, which are wet completely by surfactant solution. The capillary entry pressure is estimated by assuming that the liquid/gas interface as the gas enters is hemispherical. The critical capillary pressure for snap-off results when adjacent pendular rings contact.

TABLE 1—MEASURED AND CALCULATED ENTRY AND CRITICAL CALCULATED PRESSURES NORMALIZED BY σ/r_{bead}

	Bead Diameter (mm)	Capillary Entry Pressure	Critical Capillary Pressure	Ratio of Critical to Entry Pressure
Measurements	0.35	6.5	2.8	0.43
	0.60	5.8	3.2	0.55
	0.80	6.0	2.5	0.42
	1.68	7.5	3.8	0.51
Cubic packing	—	4.8	0.71	0.15
Hexagonal packing	—	12.8	4.1	0.32

Results. Measured and estimated capillary pressures appear in Table 1. These have been normalized by the tension of the liquid/gas interface (29.8 mN/m [29.8 dynes/cm]) divided by the bead radius. Neither dimensionless capillary pressure depends systematically on bead radius and both lie between the values calculated for cubic and hexagonal packings of spheres.

The ratio of the critical to entry capillary pressures likewise does not vary with bead radius. The average of the measured values of this ratio is about 0.5; this is above the ones calculated for both regular packings of spheres. We hereafter take the critical capillary pressure for capillary snap-off to be one-half the capillary entry pressure of the porous medium.

Drainage capillary pressure curves do not allow for snap-off, because the capillary pressure is always above the capillary entry pressure. To model snap-off, therefore, imbibition-type capillary pressure curves must be used. In this way, the capillary pressure can attain the critical value for snap-off at a gas saturation between 0 and 1.0.

Generation Rate of Foam Lamellae by Capillary Snap-Off. Fig. 4 illustrates the formation of lamellae by snap-off in a constriction. We identify the rate of generation from (1) the time for liquid to accumulate in the pore neck and snap off; (2) the time for a newly created lamella to leave the snap-off site; and (3) the time for existing, flowing lamellae to enter the active site.

To generalize the phenomenon to porous media, the capillary pressure in the pore neck is identified as the critical capillary pressure for snap-off, P_c^*, and the capillary pressure in the body is identified as the average local capillary pressure, P_c. The time for sufficient liquid to accumulate in the neck of an active site is presumed to depend inversely on the difference between these:

$$t_{so} = \frac{a}{P_c^* - P_c}, \text{ for } P_c \le P_c^* \quad \ldots\ldots\ldots\ldots\ldots\ldots\ldots\ldots (5a)$$

and

$$t_{so} = \infty, \text{ for } P_c > P_c^*. \quad \ldots\ldots\ldots\ldots\ldots\ldots\ldots\ldots (5b)$$

The time for a newly formed lamella to exit a constriction is proportional to the interstitial gas velocity,

$$t_{\text{exit}} = L_p/v_g. \quad \ldots\ldots\ldots\ldots\ldots\ldots\ldots\ldots\ldots\ldots\ldots\ldots (6)$$

Hence, the total time to form a lamella by snap-off becomes

$$t_{\text{form}} = t_{so} + t_{\text{exit}}. \quad \ldots\ldots\ldots\ldots\ldots\ldots\ldots\ldots\ldots\ldots\ldots\ldots (7)$$

The above analysis ignores existing lamellae that convect into the active site. These can remove liquid from the neck that would otherwise form new lamellae. If existing lamellae convect into the neck more frequently than lamellae can be formed, no lamellae are generated. The frequency at which existing lamellae flow into the pore neck is proportional to the product of the number of lamellae

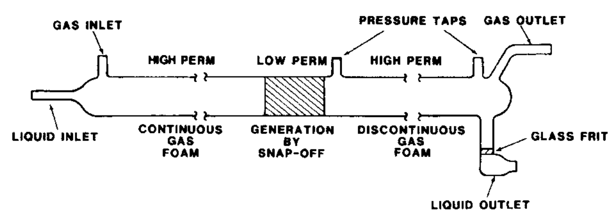

Fig. 7—Bead pack consisting of a low-permeability zone between two sections of higher permeability.

per unit length and the gas-phase velocity:

$$t_{conv}=\frac{1}{n_L v_g}. \quad (8)$$

Therefore, the frequency of generation is $1/t_{form}$ if $t_{form}<t_{conv}$ and 0 if $t_{form}\geq t_{conv}$.

To obtain the total rate of generation by snap-off, the frequency of generation per site is multiplied by the number of active sites per unit volume. The rate of generation is

$$q_f=\frac{n_n}{\dfrac{a}{P_c^*-P_c}+L_p/v_g}, \quad P_c<P_c^* \text{ and } t_{form}<t_{conv} \quad (9a)$$

and

$$q_f=0, \quad \text{otherwise}. \quad (9b)$$

The rate (1) is zero when $P_c^*-P_c$ is negative; (2) depends linearly on $P_c^*-P_c$ with slope n_n/a when $P_c^*-P_c$ is small and positive; and (3) approaches $n_n v_g/L_p$ when $P_c^*-P_c$ is large. The constraint involving t_{form} and t_{conv} shows that lamellae are generated whenever

$$\frac{1}{n_L}>L_p+\frac{a v_g}{P_c^*-P_c}, \quad (10)$$

the rate being zero otherwise. Accordingly, lamellae cannot be generated by capillary snap-off without limit. That is, the generation rate goes to zero whenever lamellae become too closely spaced.

Formulation of a One-Dimensional Simulator

To predict the behavior of one-dimensional (1D) foam displacements, a finite-difference simulator was formulated by augmenting the usual conservation equations with the population balances. As outlined in the Appendix, all equations were cast in dimensionless form. Values of the parameters used in the simulations are also recorded in the Appendix.

Mass-Conservation Equations. The mass-conservation equations were derived for 1D, two-phase, incompressible flow, including the effects of capillary pressure. Water saturation was the dependent variable:

$$\phi\frac{\partial S_w}{\partial t}+u_t\frac{\partial f_w}{\partial x}=0 \quad (11)$$

and

$$f_w=\left\{1+\frac{k}{u_t}\lambda_{rg}\left[\frac{\partial P_c}{\partial x}+g(\rho_w-\rho_g)\sin\alpha\right]\right\}\Big/(1+\lambda_{rg}/\lambda_{rw}). \quad (12)$$

These equations differ from the ones describing conventional two-phase flow only by the way gas mobility depends on foam properties.

The partial derivatives in Eqs. 11 and 12 were approximated by finite differences. Explicit, upstream weighting was used for the convection terms and implicit, central differencing was used for the capillary pressure gradient. The spatial coordinate was discretized uniformly. The fractional flow was specified at the inflow end and the capillary pressure was made zero at the outflow end. The fractional flow was constrained to be between 0 and 1.0 so that backflow could not occur at the outflow end.

The surfactant concentration was taken as uniform. To calculate the transport of surfactant requires another equation.

Population Balance. The population balance was derived for the case where capillary snap-off was the only mechanism changing bubble density. The fraction of gas flowing was taken as constant. This latter simplification removes the stationary bubble balance from the system of equations because it is coupled to the others only through x_f. A 1D form of Eq. 2 thus sufficiently describes the bubble population dynamics:

$$\phi x_f\frac{\partial(S_g n_f)}{\partial t}+u_t\frac{\partial(f_g n_f)}{\partial x}=q_{bf}. \quad (13)$$

Functional Relations. ***Relative Permeabilities.*** The functional forms used to model the apparent gas viscosity and generation rate by capillary snap-off appear in Eqs. 1 and 9, respectively. The gas relative permeability function was an exponent model reduced by the fraction of flowing gas, x_f:

$$k_{rg}=k_{rg}^o x_f(1-S_{wD})^E, \quad (14)$$

where

$$S_{wD}\equiv(S_w-S_{wr})/(1-S_{gr}-S_{wr}). \quad (15)$$

A similar expression was used to represent the liquid relative permeability,

$$k_{rw}=k_{rw}^o S_{wD}^E; \quad (16)$$

this relation does not vary with foam texture.

Capillary Pressure Function. Drainage capillary pressure curves do not permit capillary snap-off because the critical capillary pressure for snap-off is below the capillary entry pressure. Consequently, we modified an empirical capillary pressure curve so that it was zero at $S_w=1$ and reached the critical capillary pressure for snap-off at $S_w\approx 0.47$ (see the Appendix for details). The capillary pressure was inversely proportional to the square root of permeability.

The Approach Illustrated

A simulation of a 1D foam displacement in which capillary snap-off alone modified foam texture illustrates the population-balance approach to modeling foam flow in porous media.

Experimental. Inside homogeneous bead packs, moving lamellae are generated by snap-off only when the pack is tilted and gas flows upward. In this case, gravity accumulates the liquid necessary for snap-off to occur. By contrast, lamellae are often created by snap-off in heterogeneous bead packs as gas flows from a tighter into a more permeable section. Because oil reservoirs are heterogeneous, we investigated the flow and generation of foams by snap-off in packs with a step change in permeability—i.e., the first step in quantifying generation by snap-off.

Apparatus. Glass-bead packs were constructed from 1-cm [0.4-in.] -diameter glass tubing, as shown in Fig. 7. The low-permeability section consisted of 5.1 cm [2 in.] of 0.6- to 0.8-mm [0.02- to 0.03-in.] glass beads that were lightly sintered to prevent them from invading the high-permeability section. The high-permeability sections were packed with 3-mm [0.12-in.] beads. The upstream section was 25.4 cm [10 in.] long and the downstream

TABLE 2—MEASURED AND PREDICTED PRESSURE DROPS ACROSS THE DOWNSTREAM HIGH-PERMEABILITY SECTION

Section Length (cm)	f_g	Total Superficial Velocity (cm/min)	Measured Pressure Drop (kPa)	Predicted Pressure Drop (kPa)
25.4	0.9	0.51	0.34±0.21	0.34
25.4	0.8	0.51	0.62±0.34	0.48
25.4	0.8	0.76	1.03±0.34	0.5
50.8	0.9	0.51	0.76±0.34	0.69
50.8	0.8	0.51	1.1±0.48	0.96

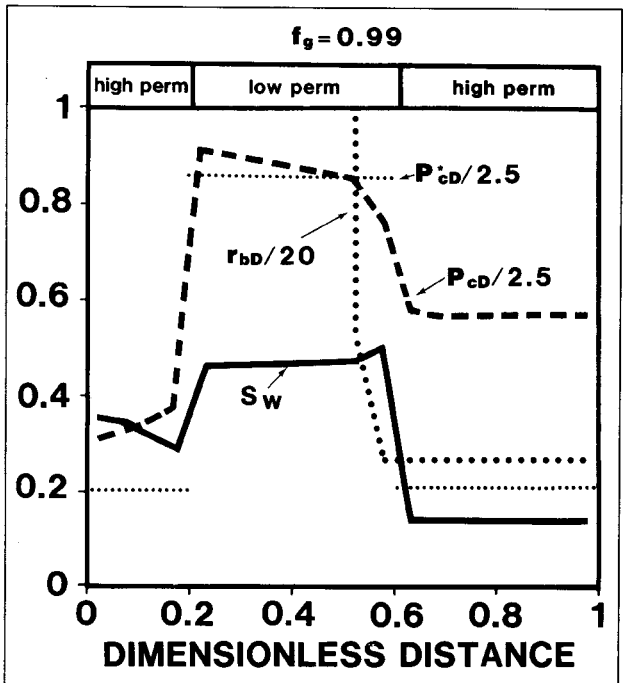

Fig. 8—Simulated profiles of liquid saturation, normalized capillary pressure, and normalized bubble size for $f_g = 0.99$.

section was either 25.4 or 50.8 cm [10 or 20 in.] long. Nitrogen and a 0.5 wt% aqueous solution of Siponate DS-10 were injected and produced separately to prevent lamellae from being generated at the inflow and outflow ends. The pressure drop across the second high-permeability section was measured with a transducer. Foam texture was observed in each section.

Experimental Results and Discussion. As gas (with or without surfactant solution) was injected (at a total superficial velocity of 0.51 cm/min [0.2 in./min]) into the pack initially filled with surfactant solution, a continuous-gas foam formed in the first high-permeability section. That is, only stationary lamellae were created there. Once gas reached the transition between the tighter section and the downstream high-permeability section, however, moving lamellae were generated and convected into the next section. These, for the most part, flowed through a single channel in the downstream section.

If the injected-gas fractional flow was below about 0.8, lamellae were steadily created near the discontinuity in permeability. At higher gas fractional flows, by contrast, lamellae were generated intermittently. That is, generation would halt for a while and then resume. The generation cycles became less frequent and foam texture coarsened as the injected-gas fractional flow was raised. In the limit where gas alone was introduced into the pack filled with surfactant solution, foam was generated intermittently with the period between generation events and the average bubble size increasing with time. Eventually, the pack became so dry that generation stopped altogether and gas flowed as a continuous phase.

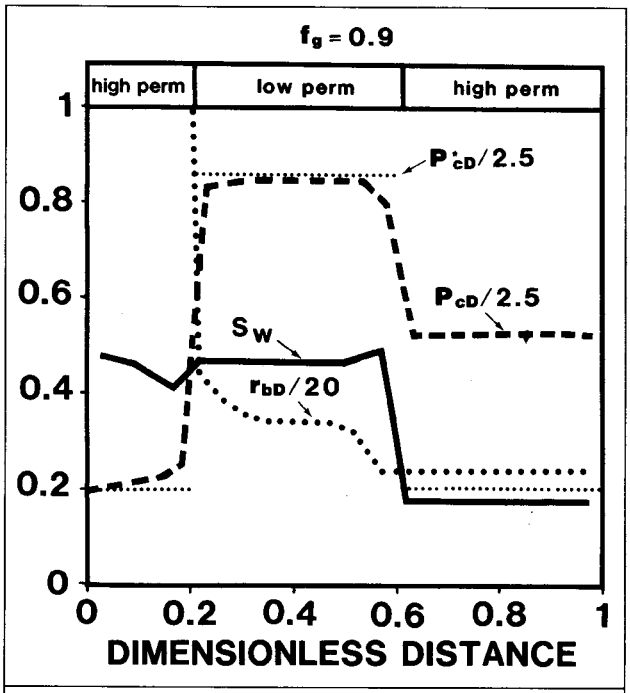

Fig. 9—Profiles of liquid saturation, capillary pressure, and bubble size simulated for $f_g = 0.9$.

We explain the intermittent generation as follows. When bubbles are generated, gas mobility is reduced and the local liquid fractional flow increases. Liquid saturation thus diminishes and capillary pressure increases until the latter exceeds the critical value for snap-off. Generation stops and the foam at the generation site is displaced by a continuous-gas phase of high mobility. Liquid then either imbibes back into the site from regions of lower capillary pressure or convects into the site if liquid is being injected. Liquid saturation rises and the capillary pressure decreases until it again drops below the value for snap-off. Generation resumes and the cycle repeats.

In several experiments run at different rates, other mechanisms also modified foam-bubble size. At a total superficial velocity of 0.34 cm/min [0.13 in./min], some of the bubbles that were generated by snap-off coalesced in the second high-permeability region. At 0.76 and 1 cm/min [0.3 and 0.4 in./min], multiple flow channels were mobilized downstream and lamellae were subdivided.

Table 2 displays the steady-state pressure drops measured across the downstream high-permeability section for the experiments in which snap-off was the only mechanism modifying the flowing bubble density. Both the average pressure drop and the magnitude of its fluctuations caused by intermittent foam generation are recorded.

Simulation. ***Comparison With Experiment.*** The parameters a, L_p, and n_n in the model for generation by capillary snap-off were evaluated by matching the predicted pressure drop to the measured value for a gas fractional flow of 0.9 and a superficial velocity of 0.51 cm/min [0.2 in./min]. Predictions with these same values of a, L_p, and n_n at other conditions are shown in Table 2.

Fluctuations in the pressure drop resulting from intermittent foam generation were also observed in the simulations. These, however, were not as large as in the experiments and were absent when the injected-gas fractional flow was below 0.9.

Interpretation. To place more gridblocks in the low-permeability section, the dimensions of the pack in the simulation were altered by eliminating some of the upstream high-permeability section. The location of the low-permeability section in the simulations is denoted in Figs. 8 and 9. Simulations with 20, 40, and 80 gridblocks determined the sensitivity to numerical accuracy. Refining the grid from 20 to 40 and from 40 to 80 gridblocks did not change the qualitative behavior but did sharpen the profiles of discontinuities and increase the pressure drop by 10 and 1%, respectively. Fluctuations in the pressure drop during transient periods also decreased as the grid was refined.

Simulations were conducted with gas fractional flows of 1.0, 0.99, 0.95, 0.9, and 0.8 being injected into packs initially filled with liquid. The cases with fractional flows less than 1.0 reached steady state after about 1.0 PV of throughput. The case of a gas fractional flow of 1.0 had a maximum pressure drop after about 1.0 PV throughput. The pressure drop declined slowly thereafter.

Simulated saturation, dimensionless capillary pressure, and dimensionless bubble-size profiles for an injected-gas fractional flow of 0.99 are shown in Fig. 8. The liquid saturation is greatest in the low-permeability section. The liquid saturation in the high-permeability section upstream is greater than in the one downstream.

The dotted horizontal lines denote the critical capillary pressure for snap-off in each section. The capillary pressure is below the critical value only near the downstream end of the tighter section. Consequently, bubbles first attain a finite size there; the bubble size remains constant in the downstream high-permeability section.

The saturation, capillary pressure, and bubble-size profiles for a gas fractional flow of 0.9 are depicted in Fig. 9. The contrast in the liquid saturation in the upstream and downstream high-permeability sections is more pronounced than in the $f_g=0.99$ case. The capillary pressure is below the critical value for snap-off throughout the tight section. Thus, the bubble-size profile indicates that bubbles are generated throughout the section.

When the gas fractional flow was reduced to 0.8, the liquid saturation in the upstream high-permeability section became high enough to generate a coarse-textured foam. Most of the foam was generated at the entrance to the low-permeability section. Additional bubbles were formed at the downstream end of the low-permeability section.

These results explain why snap-off does not generate foam in a homogeneous bead pack. If foam is generated, gas mobility decreases and the liquid saturation is reduced below the threshold required for snap-off. When there is a discontinuity in permeability, by contrast, continuity in fractional flow and capillary pressure require that the saturation be discontinuous. If the permeability increases in the flow direction, the gradient in capillary pressure in the low-permeability section retards the flow of liquid there. If enough liquid accumulates, snap-off occurs.

Conclusions

1. Texture (bubble size) is a variable that must be considered when modeling the details of the flow of foams through porous media. Texture greatly influences foam mobility and can change abruptly in the pore space.
2. Texture can be incorporated in a reservoir simulator by augmenting the usual conservation equations with balances on the densities of flowing and stationary bubbles in the foam.
3. Models for the critical capillary pressure and rate of generation of foam by capillary snap-off have been developed.
4. These models, together with one for gas mobility as a function of foam texture, have been incorporated into a 1D, finite-difference formulation of the mass-balance and population-balance equations.
5. The simulator has been used to investigate the generation and flow of foam in a bead pack with step changes in permeability.
6. A sudden increase in permeability in the flow direction can cause liquid to accumulate and snap-off to occur.

Future Work

For the approach presented here to succeed in modeling foam flow through porous media, the relationships between gas mobility, foam texture, and the variables that influence them must be established. A model for the apparent viscosity of foam under certain conditions already exists. To complete our understanding of foam mobility, a theory must also be developed to describe the fraction of the gas phase that is flowing, x_f (and thus gas-phase relative permeability) as a function of foam texture and other parameters.

Likewise, mathematical descriptions of generation and loss mechanisms like division and coalescence and of trapping and mobilization must be contrived before complex foam displacements can be modeled correctly.

Nomenclature

a = constant of proportionality in Eq. 5, Pa·s [cp]
C_k = dimensionless grouping of parameters defined in Eq. A-9
D = rate at which bubble number density changes without bubbles changing identity, bubbles/m^3·s [bubbles/ft^3-sec]
E = relative permeability exponent
f_g = fractional flow of gas
f_w = fractional flow of water
F_{rL} = ratio of equivalent capillary radius to length of pore constriction (Eq. A-19)
g = gravity acceleration=9.8 m/s^2 [32 ft/sec^2]
G = geometrical factor
G_p = pore geometrical factor in capillary pressure function, Eq. A-29
H_p = dimensionless grouping of parameters defined in Eq. A-28
J_K = number flux of bubbles caused by hydrodynamic dispersion, bubbles/m^2·s [bubbles/ft^2-sec]
k = permeability, md
L = length of porous medium, m [ft]
L_p = characteristic length of pore constriction (Eq. 6), cm [in.]
n = number density of bubbles in gas phase, bubbles/m^3 [bubbles/ft^3]
n_L = number of lamellae per unit length, lamellae/m [lamellae/ft]
n_n = number of active snap-off sites per unit volume, sites/m^3 [sites/ft^3]
N_c = capillary number
N_G = gravity number
P_c = local capillary pressure, Pa [psi]
P_c^* = critical capillary pressure for snap-off, Pa [psi]
$(P)_c$ = constant in smooth-tube viscosity expression (from Ref. 4)
P_{cDe} = dimensionless capillary entry pressure
q = net rate at which new bubbles are created in situ, bubbles/m^3·s [bubbles/ft^3-sec]
r = equivalent capillary radius of porous medium, cm [in.]
r_b = equivalent bubble radius, cm [in.]
r_{bead} = bead radius, cm [in.]
r_c = radius of curvature of gas/liquid interface, cm [in.]
R_k = ratio of endpoint relative permeabilities
S = saturation
S_{gb} = saturation at which model changed in capillary pressure function, cf. Eq. A-29
t = time, seconds
t_{exit} = time for a newly formed lamella to exit, seconds
t_{form} = time to form a lamella by snap-off, seconds
T_J = dimensionless grouping of parameters defined in Eq. A-21
u = superficial (Darcy) velocity, m/s [ft/sec]
v = interstitial velocity, m/s [ft/sec]
x = distance in Eq. 11, m [ft]
x_D = dimensionless distance
x_f = fraction of gas phase flowing
α_d = dip angle, degrees [rad]
β = parameter in smooth-tube apparent viscosity (see Ref. 4)
θ = rate at which bubbles are removed from the flowing phase by trapping, bubbles/m^3·s [bubbles/ft^3-sec]
λ_r = relative mobility, Pa·s^{-1} [cp^{-1}]
μ_g = viscosity of nonfoam gas phase, Pa·s [cp]
$\mu_{g,app}$ = apparent viscosity of gas phase, Pa·s [cp]

TABLE A-1—SIMULATION PARAMETERS THAT WERE THE SAME THROUGHOUT THE POROUS MEDIUM

Parameter	Value
$\Delta t_D/\Delta x_D$	0.05
R_k	1.5
S_{wr}	0.1
S_{gr}	0.1
E	3.4
H_p	10.0
P_{cDe}	0.4
C_k	0.365
N_G	0
N_c	7×10^{-6}
G	0.14
G_p	0.025
F_{rL}	0.441
T_J	1.63
β_D	70.7
$(P)_c$	2.0
μ_g/μ_w	0.018
S_{gb}	0.85

μ_s = smooth-tube contribution to apparent viscosity (expression is given by Hirasaki and Lawson's Eq. 40), Pa·s [cp]
μ_w = liquid-phase viscosity, Pa·s [cp]
ρ = density, kg/m^3 [lbm/ft^3]
σ = gas/liquid IFT, N/m [dynes/cm]
τ = tortuosity
ϕ = porosity
Φ = flow potential, Pa [psi]

Subscripts

b = bubble
D = dimensionless
f = flowing gas phase
g = gas
gr = residual gas
K = dispersion
ref = reference
s = stationary gas phase
so = snap-off
t = total
w = water (liquid)
wr = residual water

Acknowledgments

We thank Shell Development Co. for allowing us to publish this research. We are also grateful to J.G. Crump and J.W. Gardner for reviewing the manuscript.

References

1. Fried, A.N.: "The Foam-Drive Process for Increasing the Recovery of Oil," U.S. Bureau of Mines, Report of Investigations 5866, Dept. of Interior, Washington, DC (1961).
2. Marsden, S.S. *et al.*: "Use of Foam in Petroleum Operations," *Proc.*, Seventh World Pet. Cong., Mexico City (April 2-7, 1966) **3**, 235-42.
3. Dilgren, R.E., Deemer, A.R., and Owens, K.B.: "Laboratory Development and Field Testing of Steam Foams for Mobility Control in Heavy Oil Reservoirs," paper SPE 10774 presented at the 1980 SPE California Regional Meeting, San Francisco, March 24-26.
4. Hirasaki, G.J. and Lawson, J.B.: "Mechanisms of Foam Flow Through Porous Media—Apparent Viscosity in Smooth Capillaries," *SPEJ* (April 1985) 176-90.
5. Mast, R.F.: "Microscopic Behavior of Foam in Porous Media," paper SPE 3997 presented at the 1972 SPE Annual Meeting, San Antonio, Oct. 8-11.
6. Holm, L.W.: "The Mechanism of Gas and Liquid Flow Through Porous Media in the Presence of Foam," *SPEJ* (Dec. 1968) 359-69; *Trans.*, AIME, **243**.

TABLE A-2—SIMULATION PARAMETERS FOR DIFFERENT PERMEABILITY SECTIONS

Permeability	x_D	k_D	x_f	n_{nD}
High	0.0 to 0.2	1.0	0.9	0.2
Low	0.2 to 0.6	0.055	0.9	15.0
High	0.6 to 1.0	1.0	0.1	0.2

7. Bernard, G.G., Holm, L.W., and Jacobs, W.A.: "Effect of Foam on Trapped Gas Saturation and on Permeability of Porous Media to Water," *SPEJ* (Dec. 1965) 295-300; *Trans.*, AIME, **234**.
8. Lawson, J.B. and Reisberg, J.: "Alternate Slugs of Gas and Dilute Surfactant for Mobility Control During Chemical Flooding," paper SPE 8839 presented at the 1980 SPE/DOE Enhanced Oil Recovery Symposium, Tulsa, April 20-23.
9. Roof, J.G.: "Snap-Off of Oil Droplets in Water-Wet Pores," *SPEJ* (March 1970) 85-90; *Trans.*, AIME, **249**.
10. Falls, A.H., Lawson, J.B., and Hirasaki, G.J.: "The Role of Noncondensable Gas in Steam Foams," *JPT* (Jan. 1988) 95-104.
11. Payatakes, A.C., Ng, K.M., and Flumerfelt, R.W.: "Oil Ganglion Dynamics During Immiscible Displacement: Model Formulation," *AIChE J.* (1980) **26**, No. 3, 430-43.
12. Patzek, T.W.: "Description of Foam Flow in Porous Media by the Population Balance Method," *Proc.*, 61st Colloid and Surface Science Symposium, U. of Michigan, Ann Arbor (June 21-24, 1987).
13. Bird, R.B., Stewart, W.R., and Lightfoot, L.N.: *Transport Phenomena*, John Wiley & Sons Inc., New York City (1960) 199.

Appendix—Dimensionless Variables and Equations

Computations were made with the models, conservation equation, and population balance in dimensionless forms. In this Appendix, the dimensionless variables are defined and the values of the parameters used in the simulations given.

Mass-Conservation Equation. Eqs. 11 and 12 in dimensionless form are

$$\frac{\partial S_w}{\partial t_D}+\frac{\partial f_w}{\partial x_D}=0 \quad \text{(A-1)}$$

and

$$f_w=\left[1+x_f\frac{k_D}{\mu_D}(1-S_D)^E\left(C_k\frac{\partial P_{cD}}{\partial x_D}+N_G\right)\right]\Bigg/\left[1+x_f\frac{R_k(1-S_D)^E}{\mu_D S_D^E}\right], \quad \text{(A-2)}$$

where

$$t_D\equiv\frac{u_t t}{L\phi}, \quad \text{(A-3)}$$

$$x_D\equiv x/L, \quad \text{(A-4)}$$

$$k_D\equiv k/k_{\text{ref}}, \quad \text{(A-5)}$$

$$\mu_D\equiv\mu_{g,\text{app}}/\mu_w, \quad \text{(A-6)}$$

$$P_{cD}\equiv P_c/P_{c,\text{ref}}, \quad \text{(A-7)}$$

$$P_{c,\text{ref}}\equiv P_{cDe}\sigma\sqrt{\phi/k_{\text{ref}}}, \quad \text{(A-8)}$$

$$C_k\equiv\frac{k_{\text{ref}}k^o_{rg}P_{c,\text{ref}}}{\mu_w u_t L}, \quad \text{(A-9)}$$

$$N_G\equiv\frac{k_{\text{ref}}k^o_{rg}}{\mu_w u_t}g(\rho_w-\rho_g)\sin\alpha, \quad \text{(A-10)}$$

and

$$R_k \equiv k^o_{rg}/k^o_{rw}. \quad \text{(A-11)}$$

Values of the parameters that were the same throughout the porous medium are given in Table A-1; those that were different for the high- and low-permeability sections of the pack are listed in Table A-2.

Gas Apparent Viscosity. The dimensionless gas apparent viscosity, derived from Eq. 1, is

$$\mu_D = \mu_s/\mu_w + Gn_L r S_g x_f/(f_g N_c), \quad \text{(A-12)}$$

where

$$N_c \equiv \frac{u_t \mu_w}{\sigma\phi}. \quad \text{(A-13)}$$

The expression for μ_s is given by Eq. 40 in Ref. 4. The form appropriate to an individual-lamella foam with bubbles touching was used. To extend it to porous media, the radius of curvature was evaluated from the capillary pressure, rather than foam quality. The following relations hold:

$$n_L r = \frac{3}{4}\frac{r_D^3}{r_{bD}^3}, \quad \text{(A-14)}$$

$$r_D \equiv r/r_{\text{ref}} = \sqrt{k_D}, \quad \text{(A-15)}$$

and

$$r_{\text{ref}} \equiv \sqrt{8\tau^2 k_{\text{ref}}/\phi} \quad \text{(A-16)}$$

(from the Blake-Kozeny relation[14]).

$$r_{bD} \equiv \frac{r_b}{r_{b,\text{ref}}}\left[\left(\frac{3}{4\pi n_{fD}}\right)^{1/3}\right]\Big/F_{rL}, \quad \text{(A-17)}$$

$$n_{fD} \equiv \pi r^2_{\text{ref}} L_p n_f, \quad \text{(A-18)}$$

$$F_{rL} \equiv (r_{\text{ref}}/\pi L_p)^{1/3}, \quad \text{(A-19)}$$

$$r_{cD} \equiv (T_J P_{cD} - 1/r_D)^{-1}, \quad \text{(A-20)}$$

$$T_J \equiv P_{cDe}\sqrt{8}\,\tau, \quad \text{(A-21)}$$

and

$$\beta_D \equiv \beta/r_{\text{ref}}. \quad \text{(A-22)}$$

If the bubble density is zero, the dimensionless gas apparent viscosity is equal to the ratio of gas-phase viscosity and the water viscosity:

$$\mu_D(n_{fD}=0) = \mu_g/\mu_w. \quad \text{(A-23)}$$

Population Balance and Generation Rate by Capillary Snap-Off. The population balance in dimensionless form is

$$x_f\frac{\partial(S_g n_{fD})}{\partial t_D} + \frac{\partial(f_g n_{fD})}{\partial x_D} = q_{fD}, \quad \text{(A-24)}$$

where

$$q_{fD} \equiv \left(\frac{\pi r^2_{\text{ref}} L_p L}{u_t}\right) q_f. \quad \text{(A-25)}$$

The dimensionless rate of bubble generation is

$$q_{fD} = \frac{n_{nD}}{\dfrac{H_p}{P^*_{cD} - P_{cD}} + S_g x_f/f_g}, \; P_{cD} < P^*_{cD} \text{ and } t_{\text{form}D} < t_{\text{conv}D} \quad \text{(A-26a)}$$

and

$$q_{fD} = 0, \text{ otherwise}, \quad \text{(A-26b)}$$

where

$$n_{nD} \equiv \pi r^2_{\text{ref}} L n_n \quad \text{(A-27)}$$

and

$$H_p \equiv \frac{a u_T}{P_{c,\text{ref}} L_p \phi}. \quad \text{(A-28)}$$

Capillary Pressure Function. For high gas saturations, the dimensionless capillary pressure was described by

$$P_{cD} = \exp(-2.303 G_p \ln S_g)/\sqrt{k_D}, \quad \text{(A-29)}$$

where G_p is a pore geometrical factor. At low gas saturations, a quadratic curve that joined the above model with a continuous slope was used to extend the capillary pressure curve to a value of zero at zero gas saturation. The changes in the relationships were made at a gas saturation equal to S_{gb}.

SI Metric Conversion Factors

cp	× 1.0*	E+00	= mPa·s
in.	× 2.54*	E+00	= cm
psi	× 6.894 757	E+00	= kPa

*Conversion factor is exact.

SPERE

Original SPE manuscript received for review April 20, 1986. Paper accepted for publication July 6, 1987. Revised manuscript received Dec. 4, 1987. Paper (SPE 14961) first presented at the 1986 SPE/DOE Symposium on Enhanced Oil Recovery held in Tulsa, April 20–23.